Nuclear Materials Authority
P.O.Box 530 Maadi, Cairo, Egypt

ISSN 2314-5609
Nuclear Sciences Scientific Journal
9, 27- 53
2020
http://www.ssnma.com

GEOLOGICAL, MINERALOGICAL AND GEOCHEMICAL ASPECTS OF THE GRANITIC ROCKS AT UMM NAFIE AREA, NORTH EASTERN DESERT, EGYPT

SALAH EL-BALAKSSY; AHMED ABU STEET and AMIRA EL TOHAMY
Nuclear Materials Authority, P.O.Box:530 El –Maadi Cairo, Egypt

ABSTRACT

Wadi Umm Nafie area is located between lat. 26˚ 18` - 27˚ 05` N and long. 33˚ 23` and 33˚ 29` E. The rocks cropping out in the area are older granitoids and younger granites. The studied area displays secondary structures which are represented by joints and faults. The most predominant fault sets are trending in NE-SW, NNW-SSE and NW-SE directions. Petrographically, the older granitoids are classified as quartz diorites and the younger granites as syenogranites. The radioactivity of the syenogranites is significantly high, comparing with the older granitoids. The anomalous syenogranite (about 1x5m dimensions) exhibits equivalent uranium occurrences that vary considerably in their contents from 115.5 to 125 ppm with an average of 122.8 ppm and from 139.2 to 168.6 ppm equivalent thorium with an average of 155.4 ppm. Th-U, Zr-U, Zr-Th, , Nb-U, Nb –Th relationships show ill-defined trends, suggesting that radioelements distribution aren't controlled by accessory minerals but essentially related to the latter hydrothermal solutions. Anomalous syenogranite is affected by various phases of hydrothermal alteration processes along brittle structures, comprising hematitization, chloritization, epidotization, silicification and kaolinitization. Unusual REEs patterns and non-CHARAC ratios of isovalents confirm that the anomalous syenogranite is affected by late stage hydrothermal solutions resulting fluid-rock interaction and M-type tetrad effect. U and REEs could be leached from the sheared syenogranite at low pH conditions and precipitated in alkaline environments by hematitization process. The main minerals occur in the highly radioactive syenogranite are thorite, uranothorite, betafite, yttrocolumbite, samarskite, ishikawaite, polycrase and fergusonite, in addition to zircon, xenotime, allanite, cerite and monazite.

INTRODUCTION

The studied area represents a part of the Precambrian basement complex of the northern Eastern Desert (NED) of Egypt; it covers about 130 km^2 of crystalline basement rocks. It is bounded by lat. 26˚ 18` to 27˚ 05` N and long. 33˚ 23` to 33˚ 29` E (Fig. 1). The study area located at about 65 km west of Hurghada, Red Sea. Generally, it is characterized by rugged topography due to the presence of moderate to high mountains as Gabal (G.) Thilmah and G. Shayib Al-Banat. The area is characterized by arid climatic conditions and very rare vegetation.

There are more than twenty uranium occurrences in the northern parts of G. Gattar granite (Shalaby, 1996; El Zalaky, 2002; El Kholy el al., 2012). These occurrences were

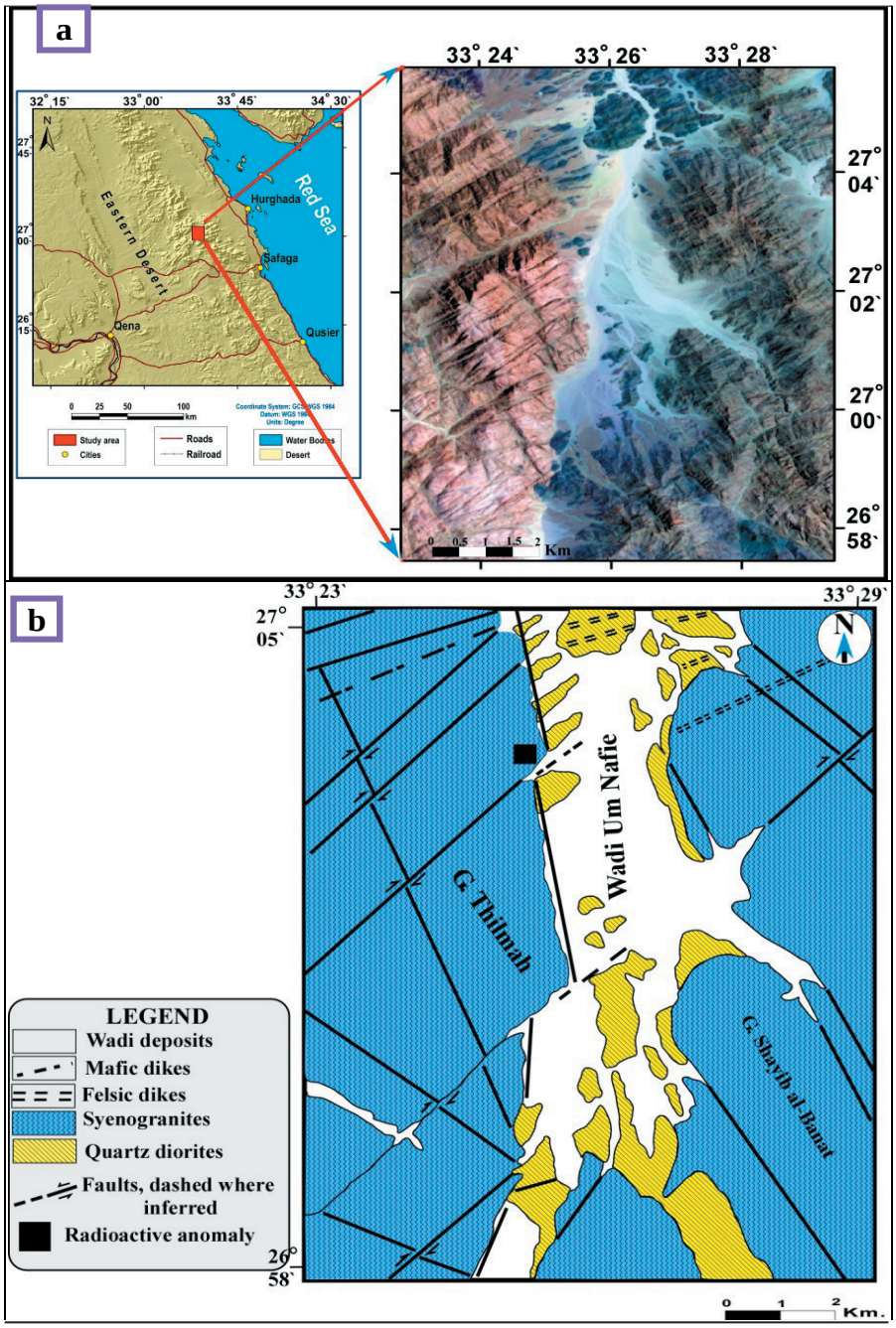

Fig. 1: a) Landsat image and b) Geologic map of Umm Nafie area

named, according to date of discovery as, G-I, G-II, G-III, G-IV, G-V…etc.

Tetrad effect from various geochemical systems is represented by irregular patterns in the normalized REE distribution and considered as indication of geochemical processes occurring in the media of mineralization. This feature known also as the 'double-double effect', 'kinked effect', or 'zigzag effect' as a new geochemical/mathematical-based tool to interpret irregular curves in normalized REE distribution patterns in a wide range of deposits (Cao et al., 2013; Lee et al., 2013; Duc-Tin and Keppler, 2015; Abedini et al., 2017; Rezaei Azizi et al., 2017; Abedini et al., 2018a). The existence of the tetrad effect in normalized REE distribution patterns can be distinguished by the presence of M and/or W forms of curves in four discrete groups of REE, first, (1) La-Ce-Pr-Nd, (2) second, Pm-Sm-Eu-Gd, third, Gd-Tb-Dy-Ho, and fourth tetrads representing four groups of rare earth elements Er-Tm-Yb-Lu, respectively (Feng et al., 2011).

The present work deals with the geology and radioactivity of the different rock types exposed at Wadi (W.)Umm Nafie area with emphasis on the younger granites (syenogranites), which constitutes the dominant part of the studied area in order to clarify their radioactive potentialities.

GEOLOGIC SETTING

A geological map at scale 1: 50,000 was prepared for the studied area (Fig. 1) using aerial photographs, TM Landsat images and extensive fieldwork. According to field studies, the rocks cropping out in the area are: 1) older granitoids (oldest), and 2) younger granites (youngest). These rocks are mostly invaded by felsic and mafic dykes, generally striking NE-SW to ENE-WSW directions.

The older granitoids are exposed as low hills and masses along the peripheries of the younger granite (Fig.2). They are dark grey in colour, medium to coarse-grained, highly weathered and highly jointed. They are characterized by low to moderate relief, exfoliation and boulder weathering. In some parts, these rocks are carbonitized and hematitized, especially in the highly fractured zones due to the effect of hydrothermal solutions.

The younger granites occur as a number of medium to high elevated outcrops. They are represented by (G.) Thilmah (eastern part of Gattar batholith) and G. Shayib Al-Banat. These younger granites intrude the older granitoids with sharp intrusive contacts; the contacts usually dip toward the older granitoids (Fig.3). Sometimes, they send several offshoots into the older granitoids. In some parts, the older granitoids occur as roof pendant over the younger granites (Fig. 4). The younger granites usually contain xenoliths of different shapes and sizes from the older granitoids. The size and number of these xenoliths increase near the contacts with the older granitoids.

The younger granites are pink in color, medium to coarse-grained, sometimes porphyritic and contain a relatively high content of mafic minerals. They are characterized by exfoliation, boulder appearance and cavernous weathering. Along joints and fault planes, these rocks show different degrees of altera-

Fig.2: Older granitoids exposed as low hills and masses along the peripheries of the younger granites, W. Umm Nafie, looking west

Fig.3: Younger granites intruded in older granitoids with sharp intrusive contact, W.Umm Nafie, looking south

Fig.5: Close up view showing kaolinitization in younger granites, W.Umm Nafie

Fig.4: Older granitoids occur as roof pendant over the younger granites, W. Umm Nafie, looking west

Fig.6: Close up view showing radioactive lens in strongly hematitized sheared granitic zone, W.Umm Nafie area

tion; the most common alteration features are hematitization, chloritization, epidotization, silicification and kaolinitization (Fig.5).

The syenogranite of G. Thilmah host a zone of radioactive anomaly (about 1x5m dimensions) which is located in the eastern part of G. Thilmah near its contact with quartz diorites. It is represented by a strongly hematitized sheared granitic zone striking NNW-SSE. This zone includes discontinuous radioactive lenses of reddish brown color (Fig. 6). The granite at this location, are medium- to fine-grained, of reddish brown color, highly sheared and kaolinitized.

Dykes, Veins and Pockets

Numerous felsic and mafic dykes of variable length and thickness are recorded traversing the studied rock types (Fig. 7). The acidic dykes stop when encountering the younger granites of Gattar batholith, indicating a relative younger age for latter. The majority of the dykes show a uniform thickness, however, few dykes are of a variable thickness along their strike. Usually, the dykes occur in parallel swarms. The main trends of these dykes are NE-SW and ENE-WSW. The study area comprises several quartz veins of different thickness and lengths as well as pegmatite pockets of different sizes.

Fig.7: Set of acidic dykes cutting in younger granites, W. Umm Nafie, looking SW

Fig. 8: Close up view showing tow conjugate shear joints in younger granite, W.Umm Nafie

Structures

The study area as a part of the northern Eastern Desert consists of Precambrian basement complex. Structures observed in the area are almost of the secondary type such as faults and joints. These secondary structures are related to the intense tectonics affecting the area. All the studied rocks are jointed, the majority of these joints are tension joints which may still empty or filled with quartz, feldspars, epidote, iron and manganese oxides. The shear joints are few and mostly parallel or sub-parallel to the main fault trends. They tend to form two complementary conjugate sets (Fig.8).

The studied area is dissected by numerous faults of different ages and trends. The fault zones are marked by fault breccia and alterations represented by hematitization, epidotization, silicification, chloritization, and kaolinitization (Fig. 9).

The attitudes of 19 major fault lines have been recorded and statistically treated (Table 1). Based on length and number proportions of the measured faults, structural analyses are represented by two rose diagrams (Fig. 10 & 11); these diagrams indicate that the common trends are NE-SW, NNW-SSE and NW-SE. This means that the structures in the studied area are following the Red Sea major faults.

Fig.9: Close up view, showing hematitization, chloritization and kaolinitization along fracture surface in younger granites, W.Umm Nafie area

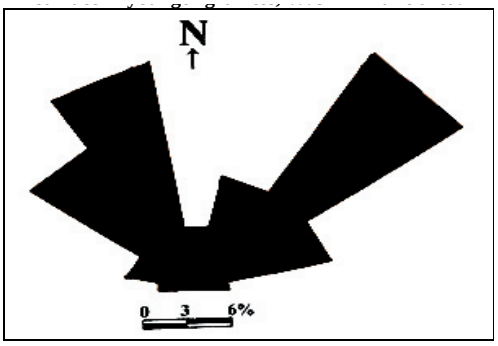

Fig.10: Rose diagrams showing the main directional trends of fault lines according to their number proportion, W.Umm Nafie area

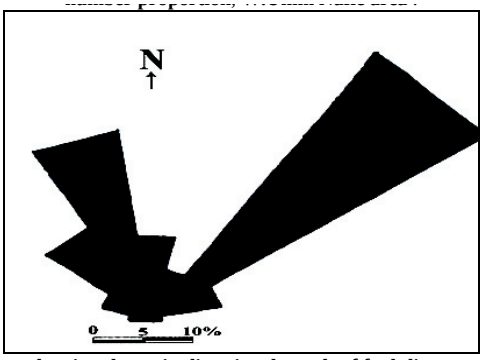

Fig.11: Rose diagrams showing the main directional trends of fault lines according to their length proportion, W.Umm Nafie area

Sampling and Methodology

To investigate the mineralogy and radioelements as well as the geochemical variations of Umm Nafie samples, five samples from the younger granites (syenogranites) were collected. Also for petrographic and radioactive studies, three samples from the older granitoids (quartz diorites) were collected. Firstly, the concerned samples were subjected to the petrographic study.

Secondly, a calibrated portable gamma-ray spectrometer (model RS-230) was used to measure the gamma-rays emitted from the daughters of U and Th and outputs the equivalent concentration of uranium (eU) and thorium (eTh) in ppm.

Thirdly, representative chemical analyses; major oxides, trace elements and 14 REE of five anomalous syenogranite were carried out using the Inductively Coupled Plasma Mass Spectrometry (ICP-MS) in the ACME Labs, Vancouver, Canada.

Finally, the anomalous syenogranite samples were subjected to heavy liquid separation (Bromoform solution (Sp.gr. 2.85g/cm^3) and picking. Consequently, the magnetic separation will be done in two steps, the first include the separation of magnetite by a hand magnet, and the second is separation of radioactive as well as some economic minerals through different magnetic susceptibilities using the Frantz Isodynamic Magnetic Separator (Model L1). Hence the obtained magnetic subfractions were carefully examined using Binocular Stereomicroscope. Thus, the identification of the different minerals in the studied rocks of W. Umm Nafie area was carried out using a Philips Environmental Scanning Electron Microscope (ESEM) model XL30 in NMA Labs.

Table (1): Frequency distribution and main trends of major faults affecting W. Umm Nafie area

Set No.	Trends of faults	Number of faults	Number proportion (N%)	Total length (km)	Length proportion (L%)
1	WNW- ESE	1	5.3	9	3.7
2	NW -SE	3	15.8	31.5	13
3	NNW-SSE	4	21	54.4	22.4
4	N-S	1	5.3	23.4	9.6
5	NNE-SSW	2	10.5	9	3.7
6	NE-SW	5	26.3	94.5	39
7	ENE-WSW	2	10.5	17.1	7.1
8	E – W	1	5.3	3.6	1.5
	Total	19	100%	242.5	100%

PETROGRAPHY

The modal composition of three samples from the older granitoids and five ones from the younger granites were tabulated in Table (2) and plotted on the QAP diagram (Streckeisen, 1976). The older granitoids plot in the quartz diorite field, while the younger granites plot in the syenogranite field (Fig. 12).

Quartz diorites are medium- to coarse-grained essentially composed of plagioclase, quartz, biotite, hornblende and minor alkali feldspars as essential minerals. Titanite, zircon, apatite and opaques represent the accessory minerals. Epidote, chlorite, sericite and kaolinite occur as secondary minerals. Plagioclase (An_{20}-An_{35}) occurs as euhedral to subhedral crystals showing lamellar twinning. Some plagioclase crystals display oscillatory zoning with an altered core and fresh rims (Fig. 13). Quartz occurs as interstitial anhedral crystals filling the spaces between the early-formed minerals indicating later stage of crystal fractionation.

Potash feldspars are very rare. Biotite occurs as irregular flakes, most of them are altered to chlorite and iron oxides especially along the cleavage planes and their margins. Hornblende found as subhedral prismatic crystals of green colour.

Syenogranite is generally porphyritic (sometimes equigranular), medium- to coarse-grained with hypidiomorphic texture. These

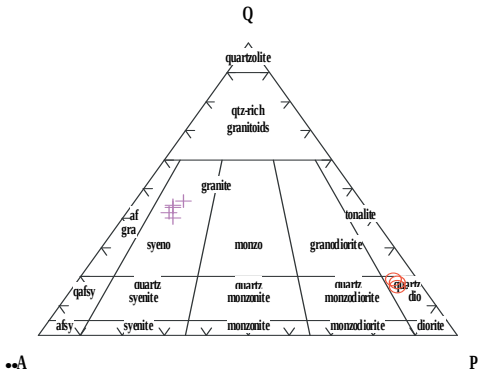

Fig. 12: Q-A-P ternary diagram (Streckeisen, 1976) for the studied quartz diorites (O) and syenogranite (+), W. Umm Nafie area

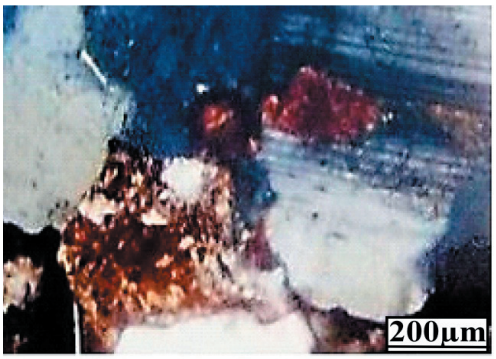

Fig. 13: Plagioclase crystal showing altered core and fresh rims, quartz diorites, XPL

Table 2: Modal analyses of the studied older granitoids (quartz diorites) and younger granites (syenogranites), W. Umm Nafie area

Rock type	Quartz diorites			Syenogranites				
Sample No.	1	2	3	4	5	6	7	8
Quartz	15.5	14.6	13.3	39.3	43.1	41.2	37.8	42.7
Plagioclase	62.8	63.9	64.9	9.9	11.3	10.1	11.9	10.1
Alkali feldspars	4.7	4.5	5.2	45.2	40.2	43.9	45.9	44.5
Biotite	7.3	8.1	8.2	2.2	2.1	1.9	1.7	1.2
Hornblende	3.8	4.3	4.5	2.3	1.6	1.7	1.9	0.8
Accessories and opaques	5.9	4.6	3.9	1.1	1.7	1.2	0.8	0.7

rocks composed of potash-feldspar, quartz, plagioclase and biotite as essential minerals. The main accessories are zircon, apatite and iron oxides whereas chlorite, sericite and kaolinite are the common alteration products.

The potash-feldspars are represented by perthites. They occur as subhedral to anhedral prismatic crystals of flame- and patchy-type (Fig. 14). Sometimes, it is altered to sericite especially at the crystal cores (Fig. 15). Quartz occurs as coarse and fine anhedral grains showing undulose extinction and cracking due to local deformation. Plagioclase occurs as subhedral prismatic crystals (Fig. 16). Occasionally, it transformed to clay minerals and carbonate (Fig. 17). Biotite found as elongated flakes and sometimes altered to chlorite. Zircon and apatite occur as prismatic crystals commonly enclosed within plagioclase, biotite and quartz.

RADIOACTIVITY

During this study, all lithological types exposed in the area of study were radiometrically surveyed. Particular attention was paid on all structural features such as contacts and faults as well as hydrothermally altered zones. Table (3) summarizes the measured equivalent uranium (eU) and equivalent thorium (eTh) contents in ppm.

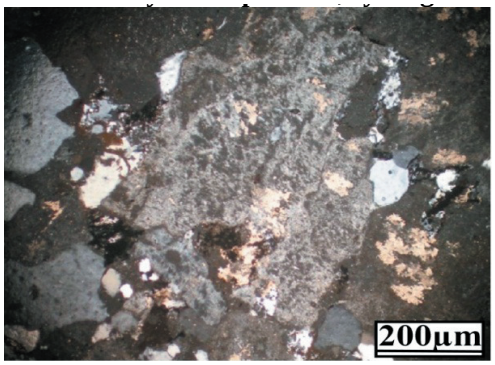

Fig. 15: The alteration of potash feldspars to sericite, syenogranite, XPL

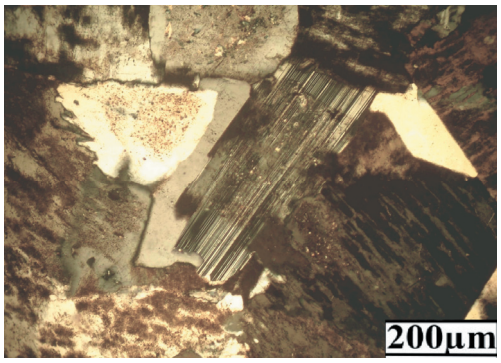

Fig.16: Subhedral crystal of plagioclase, syenogranite, XPL

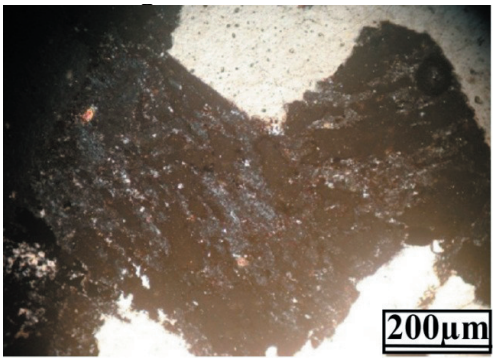

Fig. 14: Euhedral crystal of perthite, syenogranite, XPL

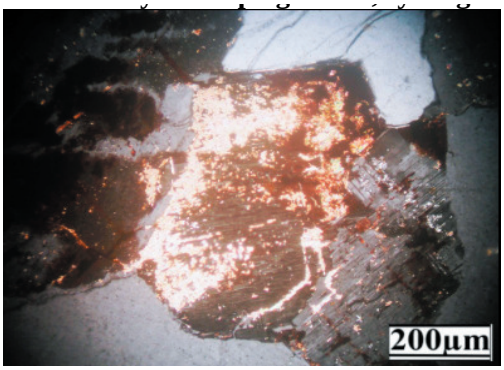

Fig. 17: Phenocryst of plagioclase transformed to carbonate, syenogranite, XPL

Table 3: eU and eTh contents (in ppm) and their ratios in the studied rock types of W. Umm Nafie area

Content	Rock type	Quartz diorites (N = 50)	Syenogranites (N = 150)	Anomalous syenogranite (N = 30)
eU (ppm)	MINIMUM	1.8	5.2	115.5
	MAXIMUM	5.3	8.4	125.0
	Average	**2.9**	**7.5**	**122.8**
eTh (ppm)	MINIMUM	5.8	9.4	139.2
	MAXIMUM	15.6	21.6	168.6
	Average	**10.4**	**16.4**	**155.4**
eU/eTh	MINIMUM	0.23	0.32	0.71
	MAXIMUM	0.31	0.52	0.98
	Average	**0.28**	**0.46**	**0.79**
eTh/eU	MINIMUM	2.32	1.02	1.10
	MAXIMUM	4.11	2.83	1.35
	Average	**3.55**	**2.19**	**1.26**

The eU of the fresh syenogranite ranges between 5.2 and 8.4 ppm with an average of 7.5 ppm and eTh from 9.4 ppm to 21.6 ppm with an average of 16.4 ppm, while at the radioactive spots in the anomalous syenogranite, the average of eU rises to 122.8 and the average eTh to155.4 ppm. The increasing in radioactivity of the anomalous syenogranite could be related to post-magmatic processes by hydrothermal solutions.

Assaf et al. (1997) concluded that uraniferous granite contain more than 18 ppm uranium. The studied anomalous syenogranite show average eU contents greater than 124 ppm. Cambon (1994) concluded that the rocks of eU/eTh average ratios greater than 0.4 are considered to be favorable environment for uranium deposits. The studied syenogranite and anomalous syenogranite show eU/eTh average ratios greater than 0.4 (Fig. 18), suggesting the favorability of the studied granites for uranium mineralization.

Normally, thorium is three times as abundant as uranium in rocks (Rogers and Adams, 1969). When this ratio is disturbed, it indicates a depletion or enrichment of uranium. In this work, syenogranite and anomalous syenogranite show eTh/eU average ratios lower than 3 (Fig. 19), suggesting addition of uranium to these rocks during secondary processes. On the other hand, quartz diorite show eTh/eU average ratios greater than 3, suggesting uranium depletion or leaching.

Geochemical Characteristics of the Anomalous Syenogranite

The distribution of the major oxides, trace elements and REEs in the anomalous syenogranite (Table 4) yielded useful information on rock/fluid interaction characteristics in addition to the physicochemical conditions of the system. During the hydrothermal alteration, nearly all the trace elements were mobilized due to dissolution or replacement of the main components and accessory minerals and new-formation of mineral phases (El Mezayen et al., 2016).

Hughes (1972) diagram indicate alkali compositions of igneous rocks, the studied altered syenogranite fall within the Na-altered (Fig.20). The altered granite sample shifted towards the greisen field on the normative Qz-

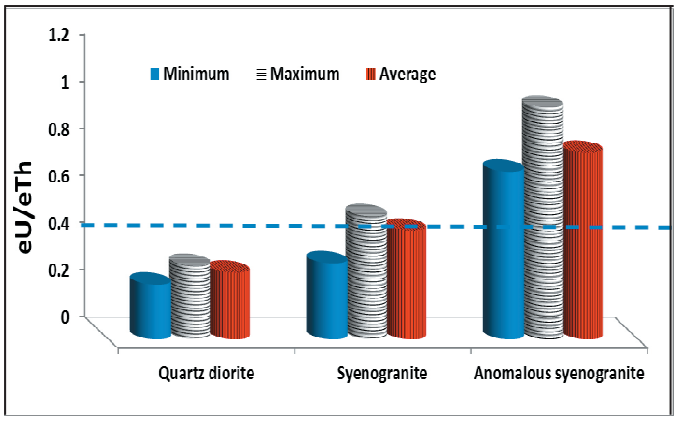

Fig. 18: eU/eTh ratios in the studied rocks, W.Umm Nafie area

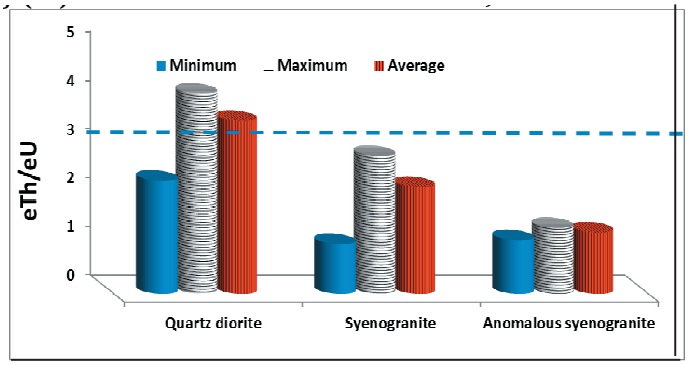

Fig. 19: eTh/eU ratios in the studied rocks, W.Umm Nafie area

Ab-Or of Stemprok (1979), (Fig.21). By using the Na_2O–K_2O variation diagram (Cuney et al., 1987), it is evident that three of the studied samples sign in the argilllation field while the other two sample fall in the silicification field (Fig.22).

The CIA values can be plotted graphically in the A-CN-K diagram in a more accurate assessment of weathering trends and conditions (Nesbitt and Young, 1984). In this diagram, all the studied samples were laid in a tight cluster near the A apex and parallel to the weathering trend (Fig.23). Al and Ga are enriched in kaolinite associated with strong chemical weathering under a warm and humid climate (Ratcliffe et al., 2010) while K and Rb are associated with illite, reflecting dry and cool climatic conditions. Consequently, sediments rich in kaolinite should have high Ga/Rb and low K_2O/Al_2O_3 ratios, whereas those rich in illite will have low Ga/ Rb and high K_2O/Al_2O_3 ratios (Roy and Roser, 2013). Ga/Rb ratios in the altered syenogranite are low (0.21) and high in K_2O/Al_2O_3 (0.28), suggesting a superiority, of illite produced during dry and cool climatic conditions (Fig.24).

Table 4: Whole chemical analyses for the studied anomalous syenogranite, W. Umm Nafie area

Elements	NA1	NA2	NA3	NA4	NA5	AV.
Major oxides (wt. %)						
SiO_2	73.5	72.7	74.6	73.8	72.9	73.5
TiO_2	0.33	0.3	0.27	0.02	0.02	0.2
Al_2O_3	12.6	12.6	12	12.5	12.7	12.5
Fe_2O_3	1.1	1.5	1.6	1.4	1.4	1.4
MnO	0.04	0.04	0.04	0.06	0.06	0.0
MgO	0.63	0.61	0.48	0.13	0.13	0.4
CaO	1.02	1.06	0.46	1.73	1.6	1.2
Na_2O	3.95	3.95	3.83	3.39	3.41	3.7
K_2O	4.94	4.5	4.16	4.9	5.1	4.7
P_2O_5	0.082	0.07	0.06	0.005	0.01	0.0
L.O.I	1.3	2.1	1.5	1.3	1.7	1.6
Total	99.49	99.43	99.00	99.24	99.03	99.2
Trace elements (ppm)						
Cr	30	68	49	58	49	50.8
Ba	71	79	75	77	75	75.4
W	5	8	6.5	7	6.5	6.6
Zr	192	186	191	188	189	189.2
Sn	42	41	41	42	41.33	41.5
As	2.2	2.3	2.25	2.27	2.25	2.3
U	116	120	130	100	125	118
Th	210	190	230	215	225	214
Sr	86	82	84	83	84	83.8
Cd	0.02	0.02	0.02	0.02	0.02	0.0
Sb	0.18	0.17	0.17	0.17	0.173	0.2
Bi	0.27	0.34	0.3	0.32	0.303	0.3
V	2	3	2.5	2.75	2.5	2.6
Be	8	7	7.5	7.25	7.5	7.5
Sc	0.8	0.7	0.75	0.73	0.75	0.7
Mo	1.3	2.56	1.9	2.2	1.92	2.0
Cu	9	12	11	12	10.6	10.9
Pb	24.38	25.73	25	25.4	25.03	25.1
Zn	88	86	87	85	87	86.6
Ni	2.5	4.4	3.45	4	3.45	3.6
Co	1.2	1.7	1.45	1.57	1.45	1.5
Y	101.4	88.4	94.9	91.6	94.9	94.2
Hf	26	22.7	24.3	23.5	24.3	24.2
Li	21.5	20.6	21.05	20.8	21.1	21.0
Rb	180.7	181.8	181.5	181	181.3	181.3
Ta	43	35	39	37	39	38.6
Nb	167	144	160	150	155.3	155.3
Cs	3	2.9	2.95	2.9	2.95	2.9
Ga	39	39.4	39.3	39.3	39.23	39.2
Se	0.3	0.4	0.35	0.37	0.35	0.3
Nb/Ta	3.88	4.11	4.10	4.05	3.98	4.02
Zr/Hf	7.38	8.19	7.86	8.00	7.78	7.82
Th/U	1.8	1.6	1.8	2.2	1.8	1.8
Rare earth elements(ppm)						
La	12.4	13.1	13	13	12.8	12.9
Ce	39	43	41	43	41	41.4
Pr	6.5	6.7	7	7	6.73	6.8
Nd	27.7	28.9	28	29	28.2	28.4
Sm	11	10.3	11	10	10.7	10.6
Eu	0.3	0.3	0.2	0.2	0.2	0.2
Gd	12.4	10.7	12	11	11.7	11.6
Tb	3.1	2.7	3	3	2.93	2.9
Dy	21.4	18.1	20	19	19.8	19.7
Ho	5.2	4.2	5	4	4.8	4.6
Er	17.7	14.8	16	16	16.2	16.1
Tm	4.2	3.4	4	4	3.87	3.9
Yb	32.8	28	30	29	31	30.2
Lu	5.9	4.7	5	5	5.2	5.2
Some calculated values						
LREEs	96.82	103	100	101	100	100.2
HREEs	102.7	86.6	95	91	95	94.1
LREE/HREE	0.94	1.19	1.05	1.11	1.05	1.06
REEs	199.5	189.6	195	192	194.7	194.2
Y/Ho	19.5	21.0	19.0	22.9	19.8	20.3
La/Y	0.12	0.15	0.14	0.14	0.13	0.14
Sm/Nd	0.40	0.36	0.39	0.34	0.38	0.37
Sr/Eu	287	273	420	415	420	363
Eu/Eu*	0.14	0.16	0.1	0.11	0.1	0.1
Ce/Ce*	1.15	1.2	1.3	1.2	1.17	1.3
T_1	1.2	1.2	1.3	1.3	1.2	1.2
T_3	1.10	1.13	1.09	1.24	1.11	1.13
T_4	1.19	1.07	1.13	1.11	1.09	1.2
T_{1-3}	1.2	1.18	1.17	1.24	1.17	1.2
T_{1-4}	1.20	1.15	1.19	1.18	1.16	1.17

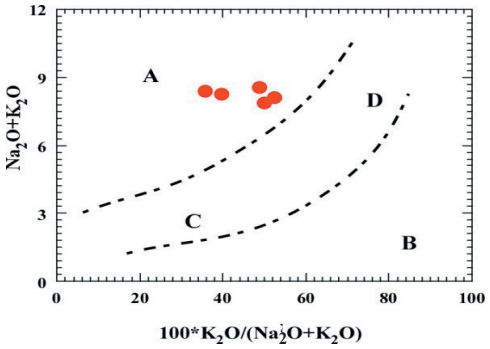

Fig.20:Total alkalis (wt.%) versus K_2O/total alkalis binary diagram of Hughes (1972).A. Na-hydrothermal alteration field; B. K-hydrothermal alteration field; C. normal igneous evolutional trend; D. normal granitic field

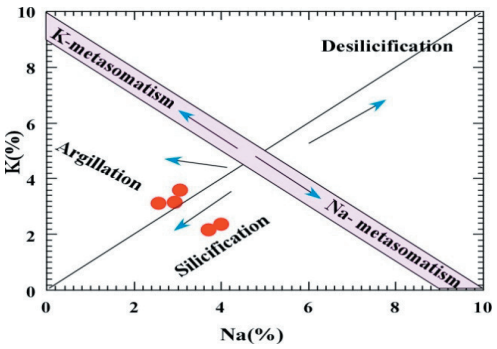

Fig. 22: Na%- K% variation diagram, showing the alteration type, after Cuney et al. (1989)

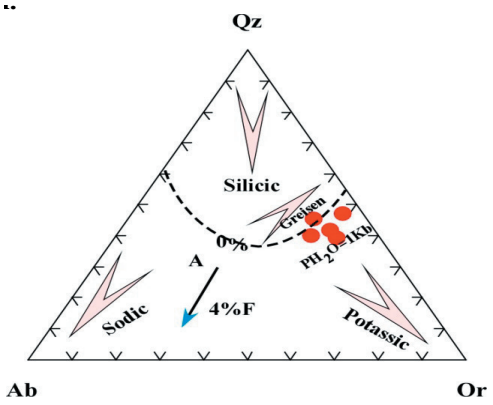

Fig. 21: Normative Q-Ab-Or ternary diagram, showing the type of alteration, after Stempork (1979). The ternary minimum for 1 kb H_2O pressure from Tuttle and Bowen (1958) and Manning (1981)

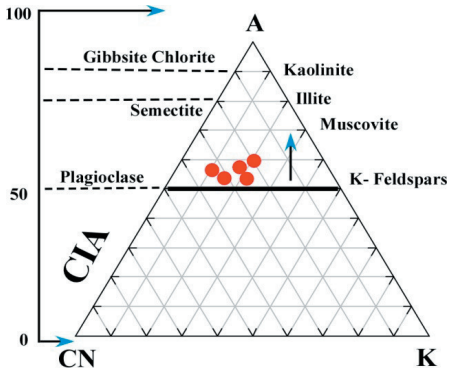

Fig.23: Al_2O_3, $(CaO+Na_2O)$, K_2O ternary diagram showing the weathering trend, after Nesbitt and Young (1984&1989)

Geochemistry of Major and Trace Elements in the Anomalous Syenogranite

Hydrothermal alteration causes mobilization of most trace elements, due to the dissolution of minerals and the formation of new mineral phases (El-Mezayen et al., 2015: Abedini et al., 2018a: Ebyan et al., 2019). The loss and gain of some elements are mainly attributed to the variations in the geochemical characteris-

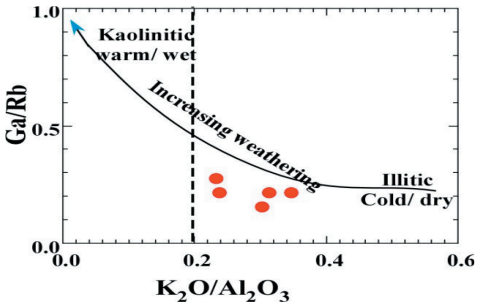

Fig.24:K_2O/Al_2O_3 vs. Ga/Rb diagram indicating degree of weathering (after Roy & Roser, 2013)

tics of the altered syenogranite. To understand the geochemical behavior of elements in the altered granites, it is recommended to normalize the pattern of such altered rocks to primitive mantle (McDonough and Sun, 1995). After that, the reference granite pattern becomes flat at unity and the relative depletion or enrichment is given by the deviations on both sides of the reference line (Figs.25a&b).

Geochemistry of major oxide is discussed in terms of gains (positive) and losses (negative) of these elements during the alteration of granites. The alteration processes show an enrichment of some major oxides such as (SiO_2, TiO_2, only in samples 1, 2& 3, Al_2O_3, and Na_2O, K_2O and P_2O_5, in most samples except sample 4) and depletion of others (TiO_2, only in samples 4&5, Fe_2O_3, MnO, MgO, CaO and P_2O_5, only in sample 4. The enrichment of Al_2O_3 could be due to the alteration of feldspars (sericitization), while the enrichment of Na_2O and K_2O are ascribed to the alkali metasomatism. The depletion of Ca could be resulted from feldspar alteration and release of these elements into the fluids responsible for alteration. The enrichment of the above major oxides is associated with the increase

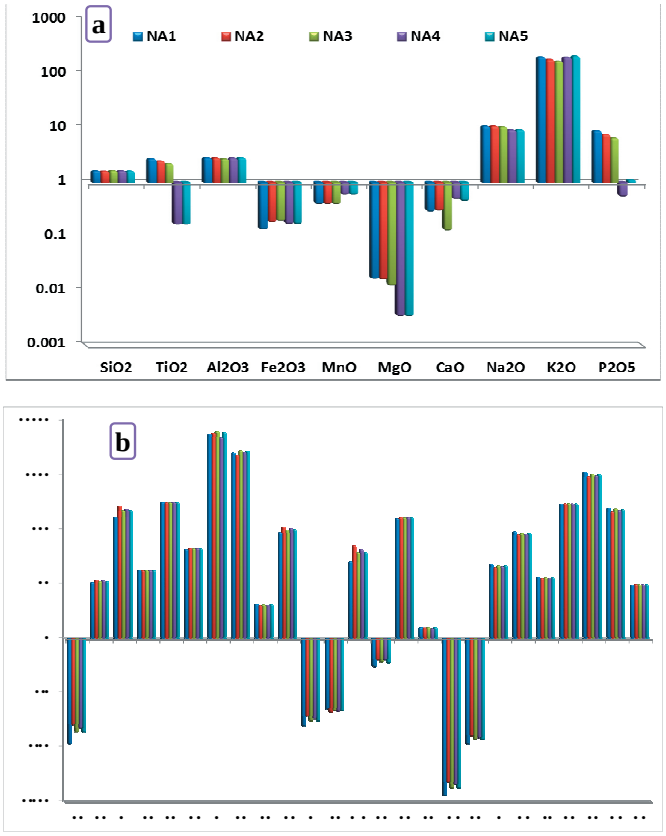

Fig.25:Histogram showing the depletion and enrichment of major oxides and trace elements of the altered syenogranite normalized to those of the primitive mantle values of Sun and McDonough (1989)

of some trace elements such as Ba, W, Zr, Sn, As, U, Th, Sr, Bi, Mo, Pb, Zn, Y, Hf, Li, Rb, Ta, Nb, Ga and decrease in the other trace elements (Cr, V, Sc, Cu, Ni and Co) relative to the primitive mantle. Rb increases with increasing K-feldspar and sericite. Ekwere (1985) indicate that Rb concentration increases in liquids rich in volatile components, being concentrated during the late magmatic differentiation. Na-metasomatism only increases Sr while K-metasomatism leads to Ba increasing (Cuney et al. 1989; El Mezayen et al. 2016). High Y, Nb and Ta contents may be ascribed to the presence of betafite, yttrocolumbite and fergusonite in the studied rocks.

Geochemistry of Isovalents

Y/Ho

Y/Ho ratios for the crust, mantle and high-temperature hydrothermal fluids are within the range of ~26–28, whereas this ratio for seawater and marine sediments increases to ~47 (Gadd et al., 2016). The studied samples have Y/Ho ratios lower than the Chondritic value (Av.20.3). The complexation with fluorine is interpreted as a major cause for Y/Ho>28, while the complexation with bicarbonate is assumed to generate Y/Ho values <28, suggesting complexation with bicarbonate.

Zr/Hf

Despite the similar behavior of Zr and Hf, the variation of the Zr/Hf ratio in a geochemical system can be attributed to fractional crystallization, hydrothermal solutions, fluids responsible for metamorphism, and tetrad effect (Bau, 1996; Tang et al., 2014; Rezaei Azizi et al., 2017; El Mezayen et al., 2019; Dostal and Chatterjee, 2000). Zr/Hf ratios of the studied samples have non-CHARAC ratios (av. 7.82) which are quite consistent with tetrad-effects of the corresponding samples. The Y/Ho and Zr/Hf ratios can reflect the physico-chemical conditions of the depositional environment. Accordingly, the non-CHARAC ratios of these pairs can be related and interpreted by tetrad-effect phenomenon (Rezaei Azizi et al., 2017).

Nb/Ta

Nb and Ta behave similarly in geochemical processes (Ballouard et al., 2016), but fractionation of Nb from Ta has been reported in various geological environments (Tartese & Boulvais 2010; Stepanov et al., 2014; Dostal et al., 2015). Although the solubility of Nb and Ta increase with fluid temperatures (Badanina et al., 2010), their solubility's in F-bearing solutions increase under reducing conditions (Zaraisky et al., 2010). Stepanov et al. (2014) demonstrated that solubility of Nb increases with temperature. This brings about high Nb/Ta ratios in high-temperature deposits. This increase can be related to destruction of biotite which preferentially has higher Nb content. On the other hand, the solubility of Nb and Ta in aqueous systems is very low (Zaraisky et al., 2010). The chondritic ratio of Nb/Ta is 17.6 ±1. The studied altered granites show non-chondritic ratios for Nb/Ta (Av. 4.02).

Rare Earth Elements (REEs)

Rare earth elements were often accepted as rather immobile elements, but more recent studies showed that they can be mobilized by hydrothermal fluids circulation (Michard and Albarede, 1986). Most REEs are transported in alkaline solutions as carbonate, sulphate or fluorine complexes. Also, Zr and Th may be mobile especially in high temperature hydrothermal environments with strong complexing agents such as fluorine, sulphide and others (Keppler H. 1993). Table (4) shows the REEs concentration of the studied anomalous syenogranite and Figure (26) shows normalized REEs patterns.

Eu, Ce Anomaly and La/Y Ratio

Europium anomaly ($Eu/Eu^{*}=Eu_N/(Sm_N\times Gd_N)^{0.5}$) are mainly controlled by plagioclase fractionation especially in felsic magmas. Thus, removal of feldspars from a felsic melt by crystal fractionation or by partial melting of a rock in which feldspars are retained in the source will give rise to negative Eu anomaly in REE patterns (Singh et al.,

2006). The Ce and Eu anomalies generally depend on Eh (fO_2) and pH of solutions during deposition processes (Abedini et al., 2017). The oxidation of Eu^{2+} converts to Eu^{3+} under higher fugacity of oxygen and is characterized by negative Eu anomalies (Tang et al., 2013).

The La/Y values, as an indicator of acidity-alkalinity, display two separate groups. The first group has higher La/Y values (>1), being indicative of alkalic conditions. The second one has relatively lower La/Y values (<1), and can be attributed to acidic conditions (Maksimovic and Pantó, 1991). All the studied samples have La/Y values (<1), suggesting acidic conditions in the environment of REEs precipitation. Therefore, the higher fugacity of oxygen in the low pH solution causes increase the amounts of Eu^{3+} in the solutions reacted with parental rocks. Under these conditions, the mineral phases precipitated from such solutions can produce negative Eu in mineral phases. Abedini et al. (2016 & 2019) suggested that a negative Eu anomaly can be attributed to low pH of fluids/solutions during geochemical processes.

Ce anomaly Ce/Ce* ($Ce/Ce^*=Ce_N/(La_N \times Pr_N)^{0.5}$) is strongly controlled by fO_2 (Dill et al., 2016). Oxidizing environments causes Ce^{3+} to be converted into Ce^{4+} with smaller ionic radii and higher charge (Kraemer et al., 2017). Ce in a tetravalent oxidation state is generally much less mobile relative to other REE^{3+}. This means that under oxidation conditions Ce^{4+} increase in the sediments and causes positive anomaly (Mongelli et al., 2014).

Ce anomaly in all samples are positive, suggests the oxidizing condition, under which the REEs were precipitated, where cerium oxidizes to its immobile Ce^{4+} state.

REE can be easily leached from weathered environments under low pH conditions and can be precipitated in alkaline environments by the presence of scavenging agents (e.g., Fe-oxides/ hydroxides) that cause their fixation (Ohta et al., 2009; Sasmaz et al., 2014, 2017). The high HREEs content relative LREEs may clarify that LREEs could be precipitated with uranium elsewhere in the sheared granites. El Feky (2011) shows the presence of mirroring between HREEs and LREEs in Gattar granites and Hammamat sediments.

Tetrad Effect

Masuda et al. (1987) classified the tetrad effect into two different types, M-and W-type (M-type in solid sample as residues and W-type in the interacting fluids as extract). The values of tetrad effect were calculated according to the quantification method of Irber (1999): $t_1 = (Ce/Ce^* \times Pr/Pr^*)$ $t_3 = (Tb/Tb^* \times Dy/Dy^*)$

$t_4 = (Tm/Tm^* \times Yb/Yb^*)$ Degree of the tetrad effect $T_{1,3} = (t_1 \times t_3)^{0.5}$

The calculated values of the tetrad effect average about 1.2. The M-shaped pattern shows $TE_i > 1.1$ and the W-shaped - $TE_i < 0.9$. The M-shaped tetrad effect has been reported from most granites and igneous systems in which crystallization and fluid-rock interactions were suggested to be the main mechanisms for producing the tetrad effect (Nardi et al., 2012).

The kinks in the REE patterns are camouflaged by prominent convex tetrad and pronounced negative Eu anomalies. The Chondrite-normalized REE patterns of studied anomalous syenogranite show M-type tetrad effect similar to that quoted by Masuda et al. (1987), (Fig. 26). T_{1-3} is higher than 1.10 with average 1.2, which clarify that there was an interaction between melt and water-haloid rich fluid when these granites are crystallized from magma.

MINERALOGY OF THE ANOMALOUS SYENOGRANITE

The heavy fractions of anomalous syenogranite samples were subjected to mineralogical investigation. The obtained analysis clarified the presence of the radio-elements (U and Th) in the structure of these minerals. The most important radioactive minerals are:

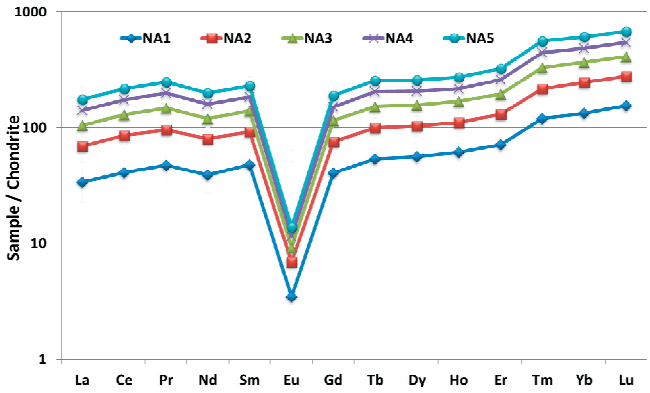

Fig. 26: Chondrite – normalized REE pattern of anomalous syenogranite, Chondrite values are taken from Sun, (1980)

Th and U-Th Minerals

Thorite (Th, U) SiO_4

Thorite is the most prevalent radioactive mineral. It usually occurs with some uranium replacing thorium. The ESEM analyses data shows that the thorite consists mainly of Th (40.5 wt. %), U (9 wt. %), Y (11.5 wt. %) and Zr (9 wt. %), (Fig.27).

Uranothorite

It is a variety of thorite (uranium variety of thorite). According to Heinrich, (1958) uranium content is usually present in amounts up to about 10% in uranothorite. The ESEM data of the studied uranothorite grains illustrated that the major elements are Th (60 wt. %) and U (14.5 wt. %) with traces of Y (Fig.28).

Nb- Ta Minerals

Betafite $(Ca,U)_2(Ti,Nb,Ta)_2O_6(OH)$

Betafite is a mineral group in the pyrochlore supergroup, with the chemical formula $(Ca,U)_2(Ti,Nb,Ta)_2O_6(OH)$. The analyses show that betafite is enriched in U (41-61 wt. %), Nb (12.3-30.3 wt. %), Ta (4-1 wt. %) with traces of Ti, Y and Yb, (Fig.29).

Yttrocolumbite $(Y, U, Fe^{2+})(Nb, Ta)O_4$

The name is derived from its yttrium content and similarity to columbite. The EDX analyses show that, Yttrocolumbite is composed mainly of Nb (36 wt. %), Ta (5 wt. %), Y (13.6 %), U+Th (10.5 wt. %) with traces of Yb (6 wt. %) (Fig.30).

Fergusonite ($YNbO_4$)

The chemical formula of fergusonite species is (Y, RE) NbO_4, where RE = rare-earth elements in solid solution with Y. Fergusonite, ideally $YNbO_4$, occurs as an accessory mineral in granitic rocks, and often combined with one or more Y, Th, Nb, Ta, Ti oxide accessory mineral (Lumpkin,1998).

The identification of this mineral is carried out by ESEM, and have Nb (37wt. %), Y (24 wt. %) and Yb (12 wt. %) with traces of U (Fig.31).

Samarskite $(Y, Fe^{3+}, Fe^{2+}, U, Th, Ca)_2 (Nb, Ta)_2O_8$

Samarskite is a radioactive with rare earth and yttrium. It is one of several rare earth oxides. The identification of this mineral is carried out by ESEM, and has Nb (37wt. %), Y

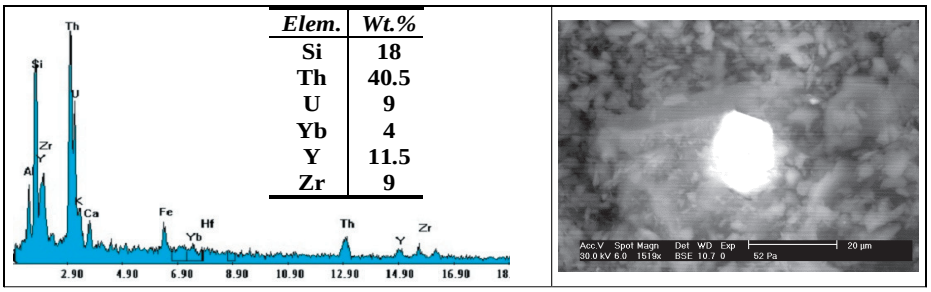

Elem.	Wt.%
Si	18
Th	40.5
U	9
Yb	4
Y	11.5
Zr	9

Fig. 27: EDX spectra and BSE image of thorite.

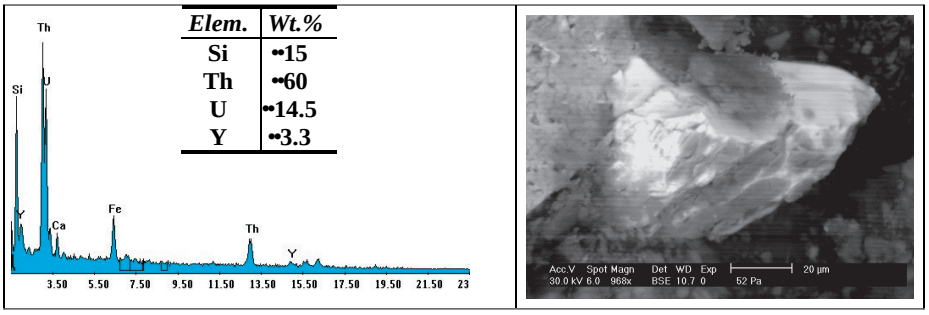

Elem.	Wt.%
Si	••15
Th	••60
U	••14.5
Y	••3.3

Fig. 28: EDX spectra and BSE image of uranothorite

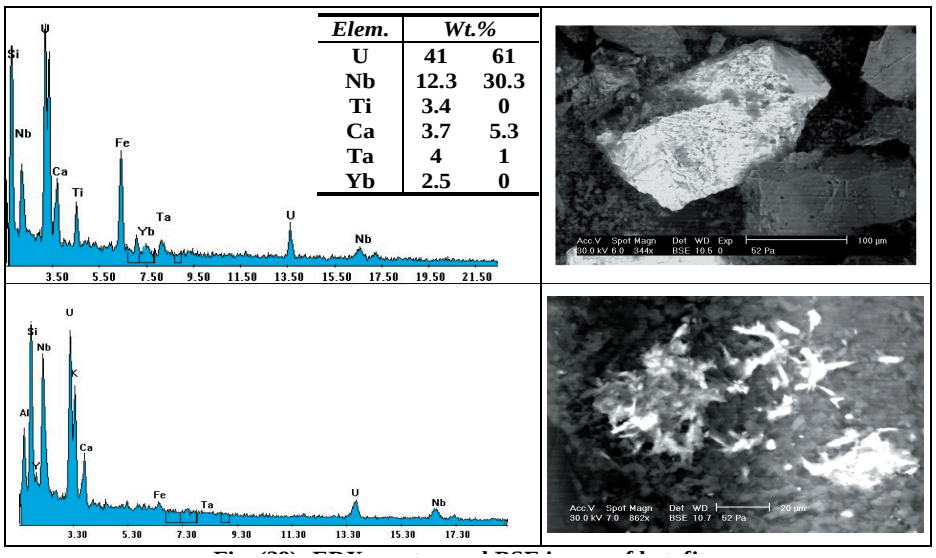

Elem.	Wt.%	
U	41	61
Nb	12.3	30.3
Ti	3.4	0
Ca	3.7	5.3
Ta	4	1
Yb	2.5	0

Fig. 29: EDX spectra and BSE image of betafite

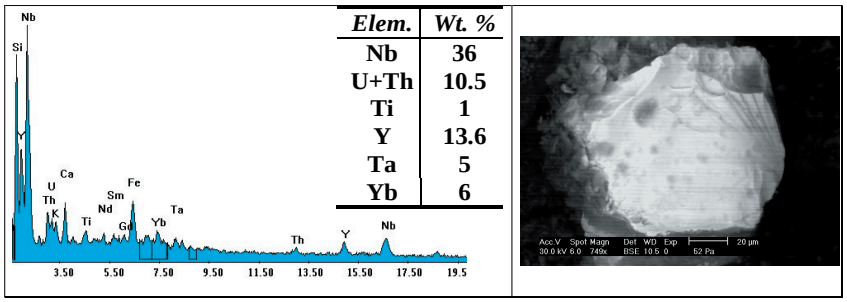

Fig. 30: EDX spectra and BSE image of yttrocolumbite

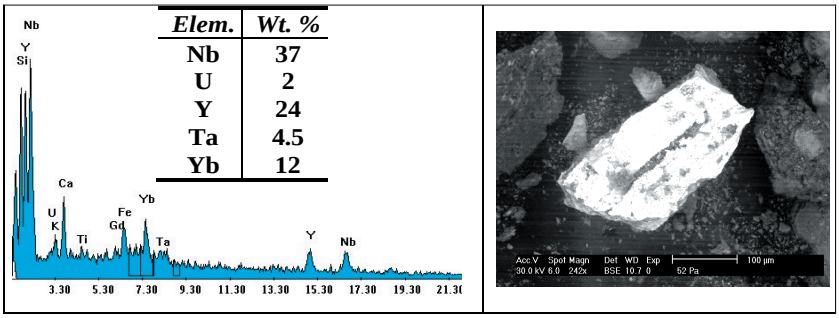

Fig. 31: EDX spectra and BSE image of fergusonite

(19wt. %), Ta (4.2 wt. %) and U+Th (12wt. %) and REEs (15.3wt. %), (Fig.32).

Ishikawaite [(U, Fe, Y, Ca) (Nb, Ta)O_4]

Cerny and Ercit, (1989) describe ishikawaite as a probable uranium-rich variety of samarskite. The ESEM data of the studied samples illustrated that ishikawaite has U (34 wt. %), Nb (30 wt. %), Ta (2.4) and Yb+Y (13.2 wt. %) (Fig.33).

Polycrase-(Y) (Y,Ca, U, Th)(Ti, Nb, Ta)$_2O_6$

It is member of the euxenite group; it is radioactive due to its uranium content (around 6%). Polycrase forms a continuous series with the niobium rich rare earth oxide euxenite. Analysis of polycrase mineral show that it is mainly composed of Nb (20.3-22 wt.%), Ti(16-15 wt.%), U+Th(12-12.3 wt.%), Ta(7-22.8 wt.%) and Y(14-16.5 wt.%) with traces of Yb(7.4-5.3 wt.%)(Fig.34).

Accessory Minerals

Zircon ($ZrSiO_4$)

Zircon occurs as euhedral six-sided or eight-sided prismatic crystals. Some of the studied zircon grains show lengthening where a high fluid content causes the period of zircon crystallization to lengthen (Pupin et al., 1979). The separated zircon forms euhedral to subhedral crystals (Fig.35).

Xenotime (YPO_4)

The EDX analyses shows that the xenotime consists mainly of Y (34.2 wt. %) and P (10 wt. %) with amounts of REEs (11.5 wt. %) (Fig.36).

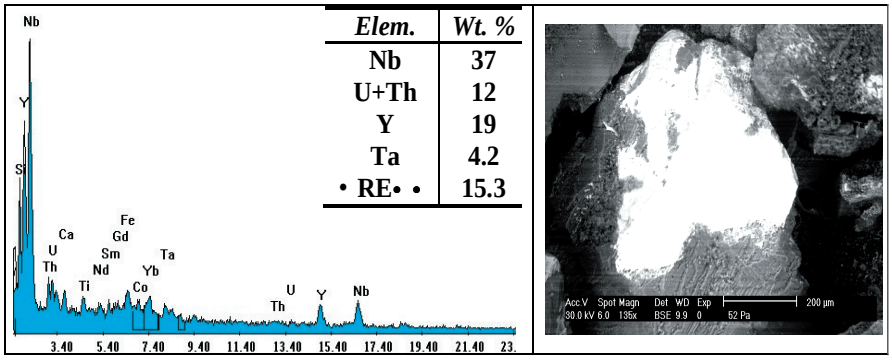

Elem.	Wt. %
Nb	37
U+Th	12
Y	19
Ta	4.2
• RE• •	15.3

Fig. 32: EDX spectra and BSE image of samarskite

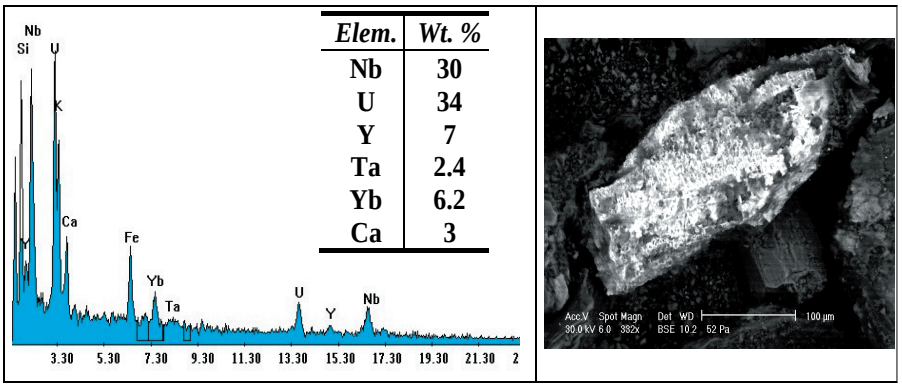

Elem.	Wt. %
Nb	30
U	34
Y	7
Ta	2.4
Yb	6.2
Ca	3

Fig. 33: EDX spectra and BSE image of ishikawaite

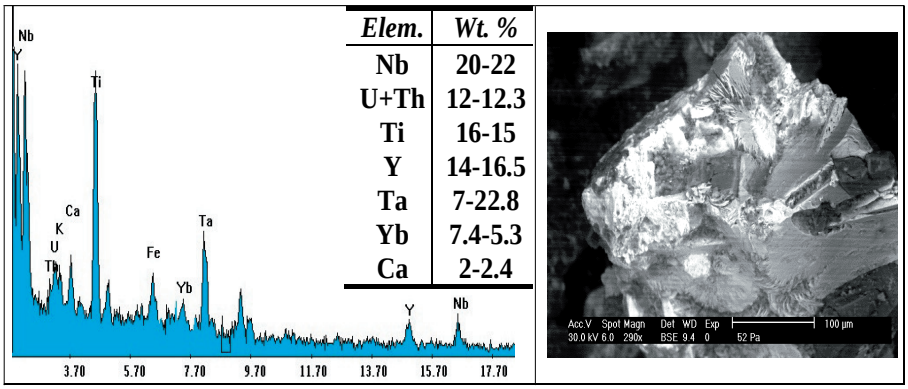

Elem.	Wt. %
Nb	20-22
U+Th	12-12.3
Ti	16-15
Y	14-16.5
Ta	7-22.8
Yb	7.4-5.3
Ca	2-2.4

Fig. 34: EDX spectra and BSE image of polycrase

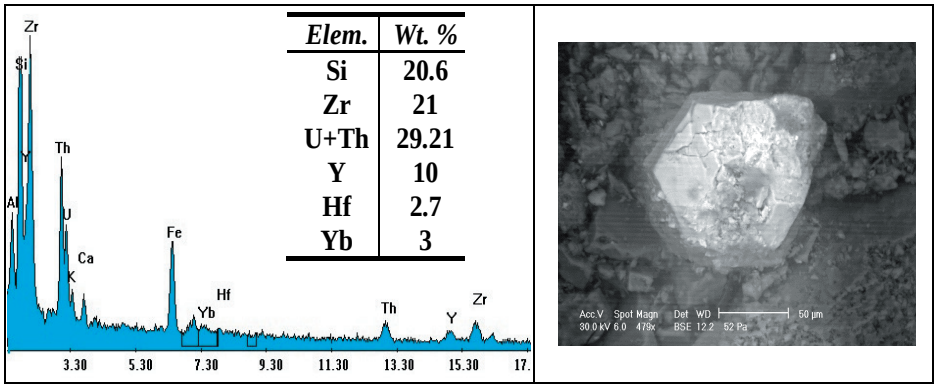

Elem.	Wt. %
Si	20.6
Zr	21
U+Th	29.21
Y	10
Hf	2.7
Yb	3

Fig. 35: EDX spectra and BSE image of zircon

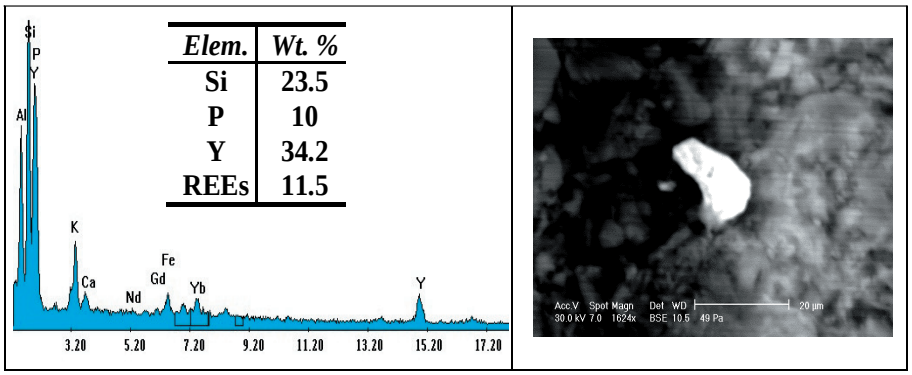

Elem.	Wt. %
Si	23.5
P	10
Y	34.2
REEs	11.5

Fig. 36: EDX spectra and BSE image of xenotime

Allanite (REEs, Ca, Y)$_2$(Al, Fe^{+++})$_3$(SiO$_4$)$_3$(OH)

The studied allanite exhibits enrichment of light rare earth elements (51.5 wt.%), (Fig.37) indicating syngenetic allanite (El-Balakssy et al., 2012).

Monazite [(Ce, La, Th, Nd, Y) PO$_4$]

Monazite is a primary ore of several light rare earth metals (66 in wt. %), most notably thorium, cerium and lanthanum. Uranium may occupy some of the REE sites (0.04 %) in monazite (Hughes et al., 1991). The EDX analyses show that monazite in the study area has REEs (45 wt. %), U+Th (30 wt. %) with traces of Y (Fig.38).

Cerite (Ce,Ca)$_9$(Mg,Fe)(SiO$_4$)$_3$(HSiO$_4$)$_4$(OH)$_3$

Cerite-(Ce) is the primary lanthanide mineral, which formed earlier than bastnaesite and allanite. The EDX analyses show that cerite in the study area has Ce (44 wt. %) (Fig.39).

CONCLUSION

Wadi Umm Nafie area displays secondary structures which are represented by joints

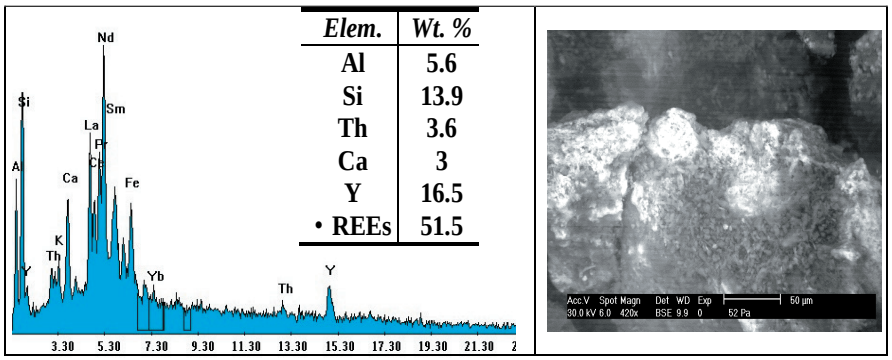

Elem.	Wt. %
Al	5.6
Si	13.9
Th	3.6
Ca	3
Y	16.5
• REEs	51.5

Fig. 37: EDX spectra and BSE image of allanite

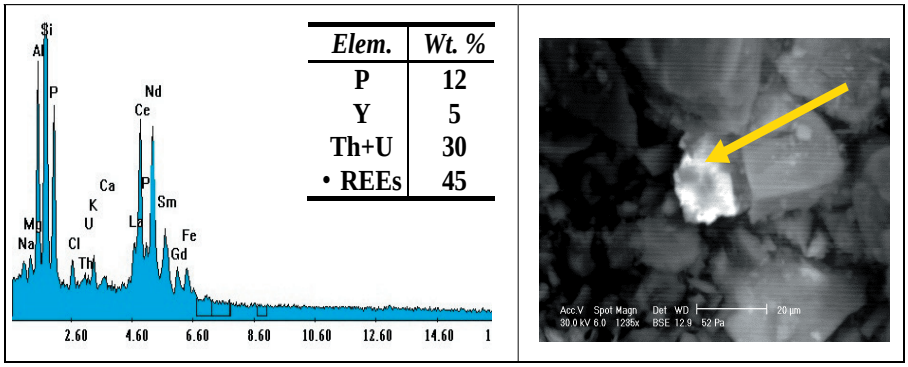

Elem.	Wt. %
P	12
Y	5
Th+U	30
• REEs	45

Fig. 38: EDX spectra and BSE image of monazite

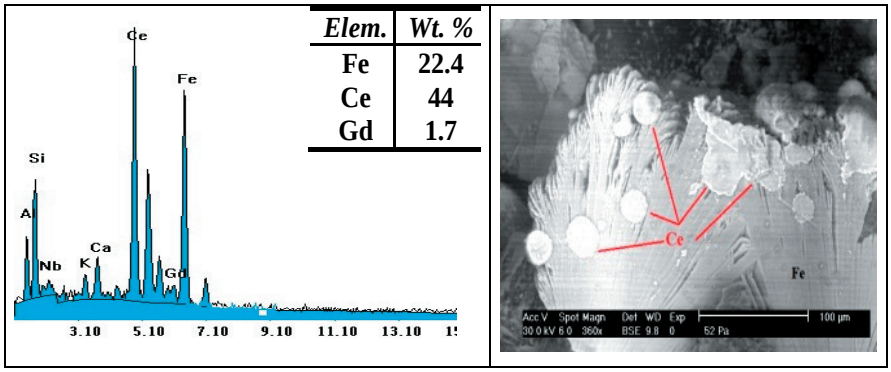

Elem.	Wt. %
Fe	22.4
Ce	44
Gd	1.7

Fig. 39: EDX spectra and BSE image of cerite

and faults, located between lat. 26˚ 18` - 27˚ 05` N and long. 33˚ 23` - 33˚ 29` E. The rocks cropping out in the area are older granitoids (oldest) and younger granites (youngest). The older granitoids are classified as quartz diorites and younger granites as syenogranites. Field radiometric survey reveals that, the radioactivity of the syenogranites is significantly high compared with the older granitoids. The syenogranites host a zone of radioactive anomaly (about 1x5m dimensions. It can be concluded that there more than one stage U and REEs mineralization, the first is enriched in the LREEs and need more investigations for its determination in the shear zone while the other enriched in HREEs and represented by the studied sheared rocks. Hydrothermal alterations are accompanied by an increase in SiO_2, TiO_2, only in samples 1, 2& 3, Al_2O_3, and Na_2O, K_2O and P_2O_5, in most samples. Ba, W, Zr, Sn, As, U, Th, Sr, Bi, Mo, Pb, Zn, Y, Hf, Li, Rb, Ta, Nb, Ga and a decrease in TiO_2, only in samples 4&5, Fe_2O_3, MnO, MgO, CaO and P_2O_5, only in sample 4, Cr, V, Sc, Cu, Ni and Co. Tetrad effects are characterized by negative Eu anomaly, unusual REEs pattern and non-CHARAC ratio of isovalents clarifying fluid-rock interaction from late hydrothermal solutions. The solution responsible for REEs mineralization in the studied granites are mainly acidic as evidenced from La/Y ratio, indicating the REEs were leached from the granite by acidic hydrothermal solutions resulting in leaching of U and rare earths and the change in pH conditions by hematitization to alkaline conditions leading to uranium and rare earth precipitation.

The anomalous syenogranite samples are characterized by presences of radioactive minerals as thorite and uranothorite; Nb-Ta minerals as (betafite, yttrocolumbite, fergusonite, samarskite, ishikawaite and polycrase); in addition to some accessory minerals as (zircon, xenotime, allanite, cerite and monazite).

Acknowledgments

The authors would like to express appreciation to Prof. Mahmoud Hany Shalaby, professor of geology, Nuclear Materials Authority, for revision and his critical comments. Also, the authors would like to express appreciation to Prof. Mohammed Galal El Feky, professor of geochemistry, Nuclear Materials Authority, for revision and his critical comments.

REFERENCES

Abedini, A.; Calagari, A.A. and Naseri, H., 2016. Mineralization and REE geochemistry of hydrothermal quartz and calcite of Helmesi vein-type copper deposite, NW Iran. Neues Jahrbuch für Geologie und Paläontologie Abhandlungen, 281, 123-134.

Abedini, A.; Calagari, A.A. and Rezaei Azizi, M., 2018a. The tetrad-effect in rare earth elements distribution patterns of titanium-rich bauxites: Evidence from the Kanigorgeh deposit, NW Iran. Journal of Geochemical Exploration, 186, 129-142.

Abedini, A.; Rezaei Azizi, M. and Calagari, A.A., 2019. Lanthanide tetrad effect in limestones: A tool to environment analysis of the Ruteh Formation, NW Iran. Acta Geodynmica et Geolmaterialia, 191(3), 229-246.

Abedini, A.; Rezaei Azizi, M.; Calagari, A.A. and Cheshmehsari, M., 2017. Rare earth element geochemistry and tetrad effects of the Dalir phosphatic shales, northern Iran. Neues Jahrbuch für Geologie und Paläontologie, Abhandlungen, 286, 169-188.

Assaf, H.S.; Mahdy, M.A. and El Afandy, A.H., 1997. Egyptian younger granite, an approach to define parameters favouring formation of uranium deposits. 3rd Conference Geochemistry, Alexandria Univ., Egypt, 409 - 420.

Badanina, E.V.; Syritso, L.F.; Volkova, E.V.; Thomas, R. and Trumbull, R.B., 2010. Composition of Li-F granite melt and its evolution during the formation of the ore-bearing Orlovka massif in Eastern Transbaikalia. Petrology, 18, 131-157.

Ballouard, C.; Poujol, M.; Boulvais, P.; Branquet, Y.; Tartèse, R. and Vigneresse, J.L., 2016. Nb-

Ta fractionation in peraluminous granites: A marker of the magmatic-hydrothermal transition. Geology, 44, 231-234.

Bau, M., 1996. Controls on the fractionation of isovalent trace elements in magmatic and aqueous systems: evidence from Y/Ho, Zr/Hf, and lanthanide tetrad effect. Contrib. Mineral. Petrol. 123, 323-333.

Cambon, A.R., 1994. Uranium deposits in granitic rocks. Notes on The National Training Course on Uranium Geology and Exploration. Organized by IAEA and NMA, 8-20 Jan. 1994.

Cao, M.J.; Zhou, Q.F.; Qin, K.Z.; Tang, D.M. and Evans, N.J., 2013. The tetrad effect and geochemistry of apatite from the Altay Koktokay No. 3 pegmatite, Xinjiang, China: implications for pegmatite petrogenesis. Mineralogy and Petrology, 107, 985-1005.

Cerny, P. and Ercit, T.S., 1989. Mineralogy of niobium and tantalum: crystal chemical relationships, para-genetic aspects and their economic implications. In Lanthanides, Tantalum, and Niobium (P. Moller, P. Cem~ and F. Saupe, eds.). Springer Verlag, Berlin, 27-79.

Cuney, M.; Leroy, J.; Valdiviezo, P. A.; Daziano, C.; Gamba, M.; Zarco, A. J.; Morello, O.; Ninci, C. and Molina, P., 1989. Geochemistry of the uranium mineralized Achala granitic complex, Argentina: comparison with Hercyman peraluminous leucogranites of Western Europe. IAEA, Vienna. T.C. 542/16.

Dill, H.G.; Luna, L.I.; Nolte, N. and Hansen, B.T., 2016. Chemical, isotopic and mineralogical characteristics of volcanogenic epithermal fluorite deposits on the Permo-Mesozoic foreland of the Andean volcanic arc in Patagonia (Argentina). Chem. Erde-Geochem., 76, 275-297.

Dostal, J. and Chatterjee, A.K., 2000. Contrasting behavior of Nb/Ta and Zr/Hf ratios in a peraluminous granitic pluton (Nova Scotia, Canada). Chem. Geol. No.163, 207-218.

Dostal, J.; Kontak, D.J.; Gerel, O.; Shellnutt, J.G., and Fayek, M., 2015. Cretaceous ongonites (topaz-bearing albite-rich microleucogranites) from Ongon Khairkhan, Central Mongolia: Products of extreme magmatic fractionation and pervasive metasomatic fluid: rock interaction. Lithos, 236-237, 173-189.

Duc-Tin, Q. and Keppler, H., 2015. Monazite and xenotime solubility in granitic melts and the origin of the lanthanide tetrad effect. Contributions to Mineralogy and Petrology, 169, 2-26.

Ebyan, O.A.; Khamis, H.A.; Baghdady, A.R.; El-Feky, M.G. and Abed, N.S., 2019. Low-temperature alteration of uranium-thorium bearing minerals and its significance in new formation of radioactive minerals in stream sediments of Wadi El-Reddah, North Eastern Desert, Egypt. Acta Geochim. https://doi.org/10.1007/s11631-019-00335-z

Ekwere, S.J., 1985. Li, F and Rb contents and Ba/Rb and Rb/Sr ratios as indicators of postmagmatic alteration and mineralisation in the granitic rocks of the Banke and Ririwai Younger granite complex, northern Nigeria. Mineral. Deposita, 20, 89-93.

El Kholy, D.M., El Husseiny, M.O., Saleh, W.H. and El Zalaky, M.A., 2012. Remote sensing, geology and geochemistry on the GVIII uranium mineralization, Gabal Gattar, North Eastern Desert, Egypt. Nucl. Sci. Sci. Jour., 1, 69-84.

El Mezayen, A.M.; El-Feky, M.G.; Omar, S.A. and Ibrahim, S. A., 2016. Geochemistry and a composite M-type with W-type of REE tetrad effect in altered granites of Abu Furad area, Central Eastern Desert, Egypt. Greener Journal of Geology and Earth Sciences, 3 (2), 013-029.

El Mezayen, A.M.; Heikal, M.A.; El-Feky, M.G.; Shahin, H.A.; Abu Zeid, I.K. and Lasheen, S.R., 2019. Petrology, geochemistry, radioactivity and M-W type rare earth element tetrads of El Sela altered granites, South Eastern Desert, Egypt. Acta Geochim., 38(1), 95-119.

El Zalaky, M.A., 2002. Interplay of plutonism, faulting and mineralization, Northern Gabal Gattar peripheral zone, North Eastern Desert, Egypt. M.Sc. Thesis, Fac. Sci., Benha Univ.,

Egypt, 178p.

EL-Balakssy, S.; Wafaa, H., and EL-Husseiny, M.O., 2012. Characterization of accessory allanite from Um Lassifa granite, Central Eastern Desert, Egypt. Al-Azhar Bull. Sci. 23,(1) 1-28.

El-Feky, M.G., 2011. Mineralogical, REE-geochemical and fluid inclusion studies on some uranium occurrences, Gabal Gattar, Northeastern Desert, Egypt. Chin. Jour. Geochem., 30, 430-443.

Feng, J.L.; Gao, S.P., and Zhang, J.F., 2011. Lanthanide tetrad effect in ferromanganese concretions and terra rossa overlying dolomite during weathering. Chemie der Erde, 71, 349-362.

Gadd, M.G.; Layton-Matthews, D. and Peter, J.M., 2016. Non-hydrothermal origin of apatite in SEDEX mineralization and host rocks of the Howard's Pass district, Yukon, Canada. American Mineralogist, 101, 1061-1071.

Heinrich, E.W., 1958. Mineralogy and Geology of Radioactive Raw Materials. McGraw Hill Book company, New York.

Hughes, C.J., 1972. Metasomatism in the late Precambrian Bull Arm formation of southeastern Newfoundland [J]. Economic Geology, 57, 240-255.

Hughes, J.M.; Cameron, M. and Mariano, A.N., 1991. Rare earth ordering and structural variations in natural rare earth bearing apatite. Amer. Mineral., 76, 1165-1173.

Irber, W., 1999. The lanthanide tetrad effect and its correlation with K/Rb, Eu/Eu*, Sr/Eu, Y/Ho, and Zr/Hf of evolving peraluminous granite suites. Geochim. et Cosmochim. Acta, 63, 489-508.

Keppler, H., 1993. Influence of fluorine on the enrichment of high field strength trace elements in granitic rocks. Contrib Mineral Petrol., 114, 479-488.

Kraemer, D.; Tepe, N.; Pourret, O. and Bau, M., 2017. Negative cerium anomalies in manganese (hydr)oxide precipitates due to cerium oxidation in the presence of dissolved siderophores. Geochimica et Cosmochimica Acta, 196, 197-208. DOI, 10.1016/j.gca.2016.09.018.

Lee, S.G.; Asahara, Y.; Tanaka, T.; Lee, S.R. and Lee, T., 2013. Geochemical significance of the Rb-Sr, La-Ce and Sm-Nd isotope systems in A-type rocks with REE tetrad patterns and negative Eu and Ce anomalies: The Cretaceous Muamsa and Weolaksan granites, South Korea. Chemie der Erde, 73, 75-88.

Lumpkin, G.R., 1998. Rare element mineralogy and internal evolution of the Rutherford pegmatite, Amelia County, Virginia: A classic locality revisited. Canadian Mineralogist, 36, 339-353.

Maksimovic, Z., Pantó, G.Y., 1991. Contribution to the geochemistry of the rare earth elements in the karst-bauxite deposits of Yugoslavia and Greece. Geoderma, 51, 93-109.

Manning, D. A. C., 1981. The effect of fluorine on liquidus phase relationships in the system Qz-Ab-Or with excess water at 1 kb. Contrib. Mineral. Petrol., 76, 206-215.

Masuda, A.; Kawakami, O.; Dohomoto, Y. and Takenaka, T., 1987. Lanthanide tetrad effects in nature: two mutually opposite types, W and M. Geochemical Journal, 21, 119-124.

McDonough, W.F. and Sun, S.S., 1995. The composition of the Earth, Chem. Geol., 120, 223-253.

Michard, A. and Albarede, F., 1986. The REE content of some hydrothermal fluid. Chem. Geol., 55, 51-60.

Mongelli, G.; Boni, M.; Buccione, R. and Sinisi, R., 2014. Geochemistry of the apulian karst bauxites (Southern Italy): Chemical fractionation and parental affinities. Ore Geology Reviews, 63, 9-21.

Nardi, L.V.S.; Formoso, M.L.L.; Jarvis, K.; Oliveira, L.; Bastos Neto, A.C. and Fontana, E., 2012. REE, Y, Nb, U, and Th contents and tetrad effect in zircon from a magmatic-hydrothermal F-rich

system of Sn-rare metalecryolite mineralized granites from the Pitinga Mine, Amazonia, Brazil. Journal of South American Earth Sciences, 33, 34-42. DOI, 10.1016/j.jsames.2011.07.004.

Nesbitt, H.W. and Young, G.M., 1984. Prediction of some weathering trends of plutonic and volcanic rocks based upon thermodynamic and kinetic consideration. Geochem. CosmoChim. Acta., 48, 1523-1534.

Nesbitt, H. W. and Young, G. M., 1989. Formation and diagenesis of weathering profiles. Jour. Geol., 97, 129-147.

Ohta, A.; Kagi, H.; Nomura, M.; Tsuno, H. and Kawabe, I., 2009. Coordination study of rare earth elements on Fe oxyhydroxide and Mn dioxides. Part II. Correspondence of structural change to irregular variations of partitioning coefficients and tetrad effect variations appearing in interatomic distances. American Mineralogist, 94, 476-486.

Pupin, J. P., Bunin, B., Tessier, M. and Turcon, G., 1979. Role de I'causulescaracteres morphologiques, et la cristallisation du zircon dans les granitoids. Bulletin Society Geology, France, 20, 721-725.

Ratcliffe, K.T.; Wright, A.M.; Montgomery, P.; Palfrey, A.; Vonk, A.;Vermeulen, J. and Barrett, M., 2010. Application of chemostratigraphy to the Mungaroo Formation, the Gorgon Field, offshore Northwest Australia. APPEA Journal (50th Anniversary Issue), 371-388.

Rezaei Azizi, M.; Abedini, A.; Alipour, S.; Niroomand, S.; Sasmaz, A. and Talaei, B., 2017. Rare earth element geochemistry and tetrad effects in fluorites: A case study from the Qahr-Abad deposit, Iran. Neues Jahrbuch für Geologie und Paläontologie, Abhandlungen, 383, 255-273.

Rogers, J.W. and Adams, J.A.S., 1969. Uranium and Thorium, In: K. H. Wedepohl (ed.), Handbook of geochemistry. Berlin, Springer-Verlag, .11 3, 92-B-1 to 92-0-8 and 90-Bb-1 to 90-00-5, 201.

Roy, D.K. and Roser, B.P., 2013. Climatic control on the composition of Carboniferous Permian Gondwana sediments, Khalaspir basin, Bangladesh. Gondwana Res., 23, 1163-1171.

Sasmaz, A.; Turkyilma, B.; Ozturk, N.; Yavuz, F. and Kumral, M., 2014. Geology and geochemistry of Middle Eocene Maden complex ferromanganese deposits from the Elazığ- Malatya region, eastern Turkey. Ore Geology Reviews, 56,352-372.

Sasmaz, M.; Obek, E. and Sasmaz, A., 2017. The accumulation of La, Ce and Y by Lemna minor and Lemna gibba in the Keban gallery water, Elazig Turkey. Water and Environment Journal, 32, 75-83.

Shalaby, M.H., 1996. Structural controls of uranium mineralizations at Gabal Gattar, north Eastern Desert. Egypt. Proc. Egypt. Acad. Sci., 46, 521-536.

Singh, A. K.; Singh, R. B., and Vallinayagan, G., 2006. Anorogenic acid volcanic rocks in the Kundal area of the Malani igneous suite, Northwestern India: geochemical and petrogenetic studies. Jour. of Asian Earth Sciences, 2, 1-14.

Stempork, M., 1979. Mineralization granites and their origin. Episodes, 3, 20-24.

Stepanov, A.; Mavrogenes, J.A.; Meffr, E, S. and David Son, P., 2014. The key role of mica during igneous concentration of tantalum. Contributions to Mineralogy and Petrology, 167, 1009-1016.

Streckeisen, A., 1976. To each plutonic rock its proper name. Earth Sci. Rev., 12, 1-33.

Sun, S.S., 1980. Lead isotopic study of young volcanic rocks from mid-ocean ridges, ocean islands and island arcs. Philosophical Transactions of the Royal Society of London, Series (A) ,297, 409-445.

Sun, S.S. and McDonough, W.F., 1989. Chemical and isotopic systematic of oceanic basalts: implications for mantle composition and processes. In Saunders A. D., Norry, M. J. (eds.), Mag-

matism in the ocean Basins. Geological Society Special Publication., 42, 313-345.

Tang, H.S.; Chen, Y.J.; Santosh, M.; Zhong, H. and Yange, T., 2013. REE geochemistry of carbonates from the Guanmenshan Formation, Liaohe Group, NE Sino-Korean. Craton: Implications for seawater compositional change during the Great Oxidation Event. Precambrian Research, 227, 316-336.

Tartese, R. and Boulvais, P., 2010. Differentiation of peraluminous leucogranites “en route” to the surface. Lithos, 114, 353-368.

Tuttle, O. F., and Bowen, N. L., 1958. Origin of Granite In The Light of Experimental Studies in The System $NaAlSi_3O_8$-$KAlSi_3O_8$-SiO_2-H_2O. Geol. Soc. Am. Em., 74, 153p.

Veksler, I.V.; Dorf Man, A.M.,; Kamenetsky, M.; Dulski, P. and Dingwell, D., 2005. Partitioning of lanthanides and Y between immiscible silicate and fluoride melts, fluorite and cryolite and the origin of the lanthanide tetrad effect in igneous systems. Geochimica et Cosmochimica Acta, 69, 2847-2860.

Zaraisky, G.P.; Korzhinskaya, V. and Kotova, N., 2010. Experimental studies of Ta_2O_5 and columbite-tantalite solubility in fluoride solutions from 300 to 550°C and 50 to 100 MPa. Miner-

الجوانب الجيولوجية والمعدنية والجيوكيميائية للصخور الجرانيتية في منطقة أم نفيع، شمال الصحراء الشرقية، مصر

صلاح صبحى البلاقصي، احمد ابو ستيت وأميرة محمد التهامي

تقع منطقة أم نفيع في شمال الصحراء الشرقية ، بين دائرتى عرض ٥٨ ` ٢٦ ° و ٥ ' ٢٧ ° شمالاً وخطي طول ٢٣ ` ٣٣ ° و ٢٩ ' ٣٣ ° شرقاً. يتميز وادي أم نفيع بطبوغرافيته الوعرة ويعتبر هذا الوادي شبه مغلقًا حيث يسمح ذلك للعديد من العناصر بالبقاء داخل الوادي بدلاً من نقلها لمسافات طويلة بعيدًا عن الصخور المصدر حيث انه محاط من الغرب بالجرانيت الحديث لجبل تيلمة وهو الجزء الشرقي من جتار.

من الدراسة البتروجرافية ، تصنف الصخور الأقدم على أنها كوارتزدايوريت، في حين أن الجرانيت الحديث يشير إلى السيانوجرانيت. والنشاط الإشعاعي للسيانوجرانيت مرتفع بشكل ملحوظ مقارنة بالجرانيتات القديمة ويمتد السيانوجرانيت الشاذ (حوالي ١ × ٥ أمتار) حيث يتراوح مكافئ اليورانيوم في محتواه من ١١٥,٥ إلى ١٢٥ جزءًا من المليون بمتوسط ١٢٢,٨ جزءًا من المليون بينما يتراوح مكافئ الثوريوم من ١٣٩,٢ إلى ١٦٨,٦ جزءًا من المليون بمتوسط ١٥٥,٤ جزءًا من المليون. بالإضافة إلى ذلك أضافت عمليات ما بعد الصهارة إلى السيانوجرانيت بعضًا من الثوريوم (٢١٤ جزء من المليون) واليورانيوم (١١٨ جزء من المليون).

وقد تأثر السينانوجرانيت بعمليات التشوه وهذا بسبب تأثير المحاليل الحارمائية على الصخر مما ادى الى تحول معظم الفلسبارات الى كاولين وسيريسيت واهم المعادن الثانوية هى الزيركون.

أظهرت الدراسة المعدنية أن السيانوجرانيت يحتوى على المعادن التالية (الثوريت، اليورانوثوريت، البيتافيت، المونازيت، الألانيت، السيريت، الإيتروكولومبيت، الفيرجسونيت، السمرسكايت، الاشكاويت، الزركون الزينوتيم).

أما من الناحية الجيوكيميائية فتظهر الأكاسيد الرئيسية تغيراً كبيراً مقارنة بمتوسط قيم القشرة الأرضية حيث يوجد إثراء فى بعض الأكاسيد مثل السيليكا، الالومنيوم والصوديوم. اما بالنسبة للعناصر الشحيحة فيوجد إثراء فى عناصر الزيركونيوم، الثوريوم، اليورانيوم، الإتريوم، النيوبيوم والهافنيوم وهذه العناصر مصاحبة لبعض المعادن مثل الزيركون حيث انه معدن مقاوم لعوامل التجوية. كما اظهرت الدراسة الجيوكيميائية ايضاً إثراءاً فى العناصر الأرضية النادرة (١٩٤ جزء من المليون).